Hypoxic pulmonary vasoconstriction does not contribute to pulmonary blood flow heterogeneity in normoxia in normal supine humans

T. J. Arai,[1] A. C. Henderson,[1] D. J. Dubowitz,[2] D. L. Levin,[2] P. J. Friedman,[2] R. B. Buxton,[2] G. K. Prisk,[1,2] and S. R. Hopkins[1,2]

[1]*Department of Medicine and* [2]*Pulmonary Imaging Laboratory, Department of Radiology, University of California, San Diego, La Jolla, California*

Submitted 12 June 2008; accepted in final form 1 December 2008

Arai TJ, Henderson AC, Dubowitz DJ, Levin DL, Friedman PJ, Buxton RB, Prisk GK, Hopkins SR. Hypoxic pulmonary vasoconstriction does not contribute to pulmonary blood flow heterogeneity in normoxia in normal supine humans. *J Appl Physiol* 106: 1057–1064, 2009. First published December 4, 2008; doi:10.1152/japplphysiol.90759.2008.—We hypothesized that some of the heterogeneity of pulmonary blood flow present in the normal human lung in normoxia is due to hypoxic pulmonary vasoconstriction (HPV). If so, mild hyperoxia would decrease the heterogeneity of pulmonary perfusion, whereas it would be increased by mild hypoxia. To test this, six healthy nonsmoking subjects underwent magnetic resonance imaging (MRI) during 20 min of breathing different oxygen concentrations through a face mask [normoxia, inspired O_2 fraction (F_{IO_2}) = 0.21; hypoxia, F_{IO_2} = 0.125; hyperoxia, F_{IO_2} = 0.30] in balanced order. Data were acquired on a 1.5-T MRI scanner during a breath hold at functional residual capacity from both coronal and sagittal slices in the right lung. Arterial spin labeling was used to quantify the spatial distribution of pulmonary blood flow in milliliters per minute per cubic centimeter and fast low-angle shot to quantify the regional proton density, allowing perfusion to be expressed as density-normalized perfusion in milliliters per minute per gram. Neither mean proton density [hypoxia, 0.46(0.18) g water/cm³; normoxia, 0.47(0.18) g water/cm³; hyperoxia, 0.48(0.17) g water/cm³; P = 0.28] nor mean density-normalized perfusion [hypoxia, 4.89(2.13) ml·min⁻¹·g⁻¹; normoxia, 4.94(1.88) ml·min⁻¹·g⁻¹; hyperoxia, 5.32(1.83) ml·min⁻¹·g⁻¹; P = 0.72] were significantly different between conditions in either imaging plane. Similarly, perfusion heterogeneity as measured by relative dispersion [hypoxia, 0.74(0.16); normoxia, 0.74(0.10); hyperoxia, 0.76(0.18); P = 0.97], fractal dimension [hypoxia, 1.21(0.04); normoxia, 1.19(0.03); hyperoxia, 1.20(0.04); P = 0.07], log normal shape parameter [hypoxia, 0.62(0.11); normoxia, 0.72(0.11); hyperoxia, 0.70(0.13); P = 0.07], and geometric standard deviation [hypoxia, 1.88(0.20); normoxia, 2.07(0.24); hyperoxia, 2.02(0.28); P = 0.11] was also not different. We conclude that HPV does not affect pulmonary perfusion heterogeneity in normoxia in the normal supine human lung.

regional pulmonary blood flow; relative dispersion; fractal dimension; log normal distribution; hyperoxia; arterial spin labeling; magnetic resonance imaging

SEVERAL STUDIES HAVE SHOWN that the distribution of pulmonary blood flow is not spatially uniform even in the normal human lung (29, 31, 33, 38, 40). The nature of the observed pulmonary blood flow heterogeneity is thought to be partially due to gravitational factors (50) influenced by posture (40) and also vascular branching structure (2, 7, 16, 17) that are partly under genetic control (15). In dogs, Glenny et al. (17) estimated that

contributions of posture and vascular structure to the total variability of pulmonary blood flow were 7.8 ± 0.6% and 83.8 ± 8.4%, respectively. In addition, dynamic factors such as hypoxic pulmonary vasoconstriction may also contribute to heterogeneity when ventilation is nonuniform. Several animal studies using either a fine aerosol inhaled into the alveoli or computed tomography have shown that ventilation is not spatially uniform (2, 36) and that the heterogeneity of ventilation is comparable to that described for blood flow (43). Hypoxic pulmonary vasoconstriction increases vascular resistance in regions of low alveolar ventilation, resulting in a correspondingly low perfusion (10). Thus any alteration in regional vascular resistance due to hypoxic pulmonary vasoconstriction in regions of low alveolar P_{O_2} ($P_{A_{O_2}}$) may affect the spatial distribution of pulmonary perfusion.

Studies evaluating the effect of hypoxia on the distribution of pulmonary blood flow have shown variable results. For example, magnetic resonance imaging (MRI) studies in normal human subjects exposed to normobaric hypoxia have been reported to show either increased perfusion heterogeneity (11) or no change (28). Similarly, in animal models using microspheres injected into the pulmonary vasculature, hypoxia results in various effects depending on species and posture. Hypoxia resulted in an increase in pulmonary perfusion heterogeneity in prone pigs and dogs (32, 45), while a decrease in heterogeneity was observed in pigs in the supine posture (27).

We hypothesized that part of the perfusion heterogeneity observed in humans within an isogravitational lung plane is due to regional hypoxic pulmonary vasoconstriction. If this were the case, breathing a mild hyperoxic gas mixture would be expected to raise local $P_{A_{O_2}}$ and abolish any localized hypoxic pulmonary vasoconstriction, resulting in a more uniform spatial distribution of pulmonary blood flow. Conversely, mild hypoxia would be expected to decrease $P_{A_{O_2}}$ throughout the lung compared with normoxia and lead to increased pulmonary blood flow heterogeneity.

To test this, we measured the distribution of pulmonary blood flow in supine healthy subjects with a functional MRI technique known as arterial spin labeling (ASL) during normoxia [inspired O_2 fraction (F_{IO_2}) = 0.21], hypoxia (F_{IO_2} = 0.125), and hyperoxia (F_{IO_2} = 0.30). These oxygen concentrations were chosen because an F_{IO_2} of 0.125 results in a $P_{A_{O_2}}$ of ~40–50 Torr, which is enough to induce hypoxic pulmonary vasoconstriction and increase pulmonary vascular resistance (3, 5). Conversely, an F_{IO_2} of 0.30 results in a $P_{A_{O_2}}$ >160 Torr,

---

which is sufficiently high to abolish the hypoxic pulmonary vasoconstriction (3, 5, 41) but is not expected to produce atelectasis (1, 48).

METHODS

Subjects. This study was approved by the Human Subjects Research Protection Program of the University of California, San Diego. Six healthy subjects [2 women, 4 men; age = 29(7) yr, height = 172(4) cm, and weight = 67(4) kg] participated after giving informed consent and undergoing screening with pulmonary and MRI safety questionnaires and a medical history and physical exam. Pulmonary function testing was performed with spirometry (VRS-2000, S&D Instrument, Doylestown, PA).

Data collection. Each subject underwent MRI scanning with a Vision 1.5-T whole body MR Scanner (Siemens Medical Systems, Erlangen, Germany), and the measurements of each subject were conducted within a single imaging session. All sequence parameters were kept within Food and Drug Administration guidelines for clinical MR examinations. Subjects were positioned supine in the scanner with a phased-array torso coil over the chest, while breathing through a full face mask (7600 series Oro-Nasal Mask, Hans Rudolph) equipped with a nonrebreathing valve (Hans Rudolph). Gases of F_{IO_2} = 0.21 (normoxia), F_{IO_2} = 0.125 (hypoxia), and F_{IO_2} = 0.30 (hyperoxia) were presented in balanced order between subjects. After a subject was allowed to breathe a particular gas for ~20 min to establish steady-state conditions, MR measurements of perfusion, proton density, and coil correction data (all described below) were acquired. We chose a 20-min duration of exposure to the gas before imaging because the initiation of hypoxic pulmonary vasoconstriction response occurs within seconds and the response to alveolar hypoxia is near maximal within 20 min in the human lung (46). A water phantom doped with gadolinium (Berlex Imaging, Magnevist, 469 mg/ml gadopentetate dimeglumine, 1:5,500 dilution) to longitudinal relaxation time (T1) and transverse relaxation time (T2) values approximating those of blood was placed next to the subject within the field of view for absolute quantification of pulmonary perfusion and proton density (see below). A single 15-mm image slice was acquired in the right lung during an 8-s breath hold at functional residual capacity, in both the sagittal and coronal planes, for each inspired oxygen concentration. Data were acquired in triplicate for each slice and F_{IO_2}, and the results were averaged after quantification.

Quantification of cardiac output with cine phase contrast. Cardiac output was estimated from the left ventricular output measured as volume of blood flowing in the aorta during each cardiac cycle, using through-plane velocity encoding for the data acquisition (14). The flow volume per cardiac cycle was calculated as the mean forward velocity through a region of interest (ROI) positioned distal to the aortic valve, multiplied by the cross-sectional area of the ROI on each cine frame. This was then multiplied by the heart rate to give a cardiac output in milliliters per minute.

Correction for coil inhomogeneity. To maximize the signal-to-noise ratio in the pulmonary perfusion and proton density data (described below), a torso coil was used, which has substantially higher gain than the body coil built into the scanner. With paired density images from the homogeneous body coil and the inhomogeneous torso coil, all blood flow and density images were corrected for coil inhomogeneity on a subject-by-subject basis as previously described (29). This coil inhomogeneity profile is essentially constant across all measurements for a given subject, as evidenced by the close relationship between two coil profiles in the same subject (R = 0.99).

Quantification of regional pulmonary perfusion with ASL. Regional pulmonary blood flow was assessed with a two-dimensional ASL-FAIRER sequence with a half-Fourier acquisition single-shot turbo spin-echo (HASTE) imaging scheme (4). During each measurement, two cardiac-gated images of each lung slice are acquired during a single breath hold. The signal of blood is prepared in a different way

in the two images. In one image, the magnetization of the blood and tissue both inside and outside the imaged section is inverted, resulting in very low signal from both blood and tissue when the image is acquired ~80% of one R-R interval later. In the second image, the inversion is applied only to the imaged slice, and after another pause of ~80% of the R-R interval the second image is acquired. This second selective inversion has the result that any inflow of blood from outside that slice has a strong MR signal. When the two images are subtracted, canceling the stationary signal, the result is a quantitative map of blood delivered to the imaging plane from one systolic ejection period. The 15-mm-thick image slices have a field of view of 40 cm × 40 cm and a resolution of 256 × 128 pixels; therefore, voxels of ~1.5 × 3 × 15 mm (~0.07 cm³) were obtained in each plane. These ASL image files were later resized during postprocessing to match the voxel size of the fast low-angle shot (FLASH) proton density images (3 × 3 × 15 mm, giving an effective resolution of ~0.14 cm³) described below with bilinear interpolation in MATLAB (MathWorks, Natick, MA). Once the subtracted ASL image was corrected for coil inhomogeneity (29), pulmonary blood flow was quantified in milliliters per minute per cubic centimeter by using the R-R interval, inversion time (TI = 600–800 ms), echo time (TE = 36 ms), and the doped water phantom with T1 and T2 matched to blood, as previously reported (29). The signal-to-noise ratio of ASL subtracted images averaged 13.4(8.2).

Quantification of regional lung density. In addition to the ASL images, a proton density image was acquired in the same image slice with a FLASH sequence during a separate breath hold. Sequence parameters were TR = 6 ms, TE = 0.9 ms, flip angle (θ) = 4°, slice thickness = 15 mm, and image size 128 × 128. In each image so obtained, the resulting signal after correction for coil inhomogeneity in each voxel was referenced to the signal derived from the water phantom (which is by definition 100% water) to obtain regional lung proton (water) density in units of grams of water per cubic centimeter of lung. The resulting proton density was then calculated by correcting the signal for the rapid T2* decay of signal from the lungs based on published values of T2* [1.43(0.41) ms; Ref. 24]. For simplicity, this proton density, which reflects both tissue and blood, is subsequently referred to in this report as density.

Density-normalized perfusion. Perfusion expressed in units of milliliters per minute per gram of water can be approximated by dividing the image acquired by ASL, which has the units of milliliters per minute per cubic centimeter of lung, by the FLASH image of proton density (in g water/cm³ lung) to give perfusion in milliliters per minute per gram of lung (tissue + blood). A mutual information-based technique that included translation and rotation was utilized to register the two ASL and FLASH images (29, 42), and then the ASL perfusion image was divided by the FLASH proton density image on a voxel-by-voxel basis. To the extent that regional lung density is reflected by the water content, this density-normalized perfusion then reflects perfusion in milliliters per minute per gram of lung.

Data analysis. For each image acquired as described above (lung proton density and density-normalized perfusion), the data were analyzed in the following manner. For each image, mean density and density-normalized perfusion were calculated. In addition, to compare the effect of different inspired oxygen concentrations on perfusion heterogeneity, four different indexes of perfusion heterogeneity were calculated in both coronal and sagittal planes. These were *1)* relative dispersion, also known as the coefficient of variation, a global scale of heterogeneity defined as the ratio of the standard deviation to the mean perfusion where the larger the relative dispersion, the more heterogeneous the distribution (21); *2)* fractal dimension (D_s), an index of the spatial heterogeneity that is scale independent, where fractal dimension varies between 1.0 (homogeneous) and 1.5 (spatially random) (19); and *3)* the shape parameter and *4)* a geometric standard deviation, also global scales of heterogeneity but based on log normal model distribution (34).

In sagittal slices, the effect of different inspired oxygen concentrations on the vertical distribution of density-normalized perfusion was also measured. The lung of each subject was divided in the anterior-posterior direction into three regions: dependent, middle, and nondependent. Mean density-normalized perfusion of each region was compared for the different inspired oxygen concentrations.

ANOVA (Statview 5.0, SAS Institute, Cary, NC) for repeated measures was used to statistically evaluate changes in the major dependent variables over the three inspired oxygen concentrations (3 levels: hypoxia, normoxia, and hyperoxia). Dependent variables for this analysis were lung density, as measured by FLASH in units of grams of water per cubic centimeter of lung, and density-normalized perfusion (ASL/FLASH, $ml \cdot min^{-1} \cdot g^{-1}$) and associated measurements of perfusion heterogeneity. Where overall significance occurred, post hoc testing was conducted with Student's t-testing. All data are presented as means(SD); the null hypothesis (no effect) was rejected for $P < 0.05$, two-tailed.

RESULTS

Six healthy subjects participated in this study (4 men, 2 women) after giving informed consent. All of the pulmonary function data were within normal limits [forced vital capacity (FVC) = 5.0(0.8) liters, FVC % predicted = 101(8), forced expiratory volume in 1 s (FEV_1) = 4.1(0.6) liters, FEV_1 % predicted = 101(8), FEV_1/FVC = 83(4), and FEV_1/FVC % predicted = 98(4)]. Physiological data for each inspired oxygen concentration are shown in Table 1. As expected, arterial oxygen saturation measured by pulse oximetry (Sp_{O_2}) was significantly reduced by hypoxia ($P < 0.001$) but unchanged ($P = 0.73$) by hyperoxia, compared with normoxia [hypoxia, 84.8(5.4)%; normoxia, 97.3(1.2)%; hyperoxia, 97.9(0.9)%]. Heart rate was significantly increased during hypoxia ($P < 0.05$) but unchanged during hyperoxia ($P = 0.67$), compared with normoxia [hypoxia, 64(8); normoxia, 58(8); hyperoxia, 57(7)]. Cardiac output measured by cine phase contrast showed a small increase in hypoxia compared with normoxia and hyperoxia, but this was not statistically significant [hypoxia, 6.0(0.8) l/min; normoxia, 5.4(0.9) l/min; hyperoxia, 5.5(1.6) l/min; $P = 0.29$].

Figure 1 shows the distribution of pulmonary perfusion, proton density, and density-normalized perfusion during normoxia in a sagittal (Fig. 1, *A1*, *B1*, and *C1*) and a coronal (Fig. 1, *A2*, *B2*, and *C2*) slice from a representative subject. Images of the coronal slice are shown on the bottom and images of the sagittal slice are shown on top. Images in Fig. 1*A* represent a pulmonary blood flow map in which the signal intensity of the images scales as a function of perfusion (ml blood $\cdot min^{-1} \cdot cm^{-3}$) as measured by ASL (Fig. 1, *A1* and *A2*). Images in Fig. 1*B* represent the proton density map measured by FLASH (Fig. 1,

B1 and *B2*), with signal intensity proportional to proton density (g water/cm^3). Images in Fig. 1*C* are density-normalized perfusion data (Fig. 1, *C1* and *C2*), which are obtained by division of the ASL perfusion image by the FLASH proton density image ($ml \cdot min^{-1} \cdot g^{-1}$).

Mean density and density-normalized perfusion data are given in Fig. 2. Mean proton density was greater in the coronal than in the sagittal plane, reflecting the dependent location of the coronal plane that was imaged. These changes did not reach statistical significance [coronal, 0.55(0.20) g water/cm^3; sagittal 0.40(0.09) g water/cm^3; $P = 0.07$; Fig. 2*A*]. The mean proton density was not altered by the different concentrations of oxygen [hypoxia, 0.46(0.18) g water/cm^3; normoxia, 0.47(0.18) g water/cm^3; hyperoxia, 0.48(0.17) g water/cm^3; $P = 0.28$; Fig. 2*A*]. Mean density-normalized perfusion in the sagittal plane was significantly greater than in the coronal plane [coronal, 3.89(1.12) $ml \cdot min^{-1} \cdot g^{-1}$; sagittal, 6.21(1.86) $ml \cdot min^{-1} \cdot g^{-1}$, $P < 0.05$; Fig. 2*B*] and was unchanged by inspired oxygen concentration [hypoxia, 4.89(2.13) $ml \cdot min^{-1} \cdot g^{-1}$; normoxia, 4.94(1.88) $ml \cdot min^{-1} \cdot g^{-1}$; hyperoxia, 5.32(1.83) $ml \cdot min^{-1} \cdot g^{-1}$; $P = 0.72$; Fig. 2*B*].

Figure 3 shows the effect of different inspired oxygen concentrations and lung slice orientations on indexes of pulmonary blood flow heterogeneity. The relative dispersion was not altered by orientation or oxygen concentrations in either coronal or sagittal planes [orientation: coronal 0.73(0.13), sagittal 0.77(0.16) ($P = 0.16$); $F_{I_{O_2}}$: hypoxia 0.74(0.16), normoxia 0.74(0.10) hyperoxia, 0.76(0.18) ($P = 0.97$); Fig. 3*A*]. Similarly, the fractal dimension D_s was not different between coronal and sagittal planes and between inspired oxygen concentrations [orientation: coronal 1.19(0.04), sagittal 1.21(0.03) ($P = 0.17$); $F_{I_{O_2}}$: hypoxia 1.21(0.04), normoxia 1.19(0.03), hyperoxia 1.20(0.04) ($P = 0.07$); Fig. 3*B*]. The shape parameter of log normal model distributions [orientation: coronal 0.68(0.11), sagittal 0.68(0.12)($P = 0.98$); $F_{I_{O_2}}$: hypoxia 0.62(0.11), normoxia 0.72(0.11), hyperoxia 0.70(0.13) ($P = 0.07$); Fig. 3*C*] and geometric standard deviation [orientation: coronal 1.99(0.25), sagittal 1.99(0.25) ($P = 1.00$); $F_{I_{O_2}}$: hypoxia 1.88(0.20), normoxia 2.07(0.24), hyperoxia 2.02(0.28) ($P = 0.11$); Fig. 3*D*] also did not show any difference between orientations or inspired oxygen concentrations.

Figure 4 shows vertical distribution of density-normalized perfusion into three regions: dependent, middle, and nondependent [dependent, 5.21(1.86) $ml \cdot min^{-1} \cdot g^{-1}$; middle, 7.49(2.31) $ml \cdot min^{-1} \cdot g^{-1}$; nondependent, 5.74(1.59) $ml \cdot min^{-1} \cdot g^{-1}$]. Density-normalized perfusion in the middle region was significantly greater than in either the dependent or the nondependent region ($P < 0.05$) for all inspired oxygen concentrations. However, no significant difference was observed between dependent and nondependent parts of the lung ($P = 0.278$). Inspired oxygen concentration did not affect the vertical distribution of density-normalized perfusion [hypoxia, 5.82(2.34) $ml \cdot min^{-1} \cdot g^{-1}$; normoxia, 6.04(2.16) $ml \cdot min^{-1} \cdot g^{-1}$; hyperoxia, 6.58(1.98) $ml \cdot min^{-1} \cdot g^{-1}$; $P = 0.39$]. There was also no significant interaction effect between the three regions and inspired oxygen concentration ($P = 0.51$).

DISCUSSION

The results of this MRI study indicate that in normoxia, hypoxic pulmonary vasoconstriction does not have a signifi-

Table 1. *Physiological data for each inspired oxygen concentration*

| | Oxygen Concentration | | | |
	Hypoxia (12.5%)	Normoxia (21%)	Hyperoxia (30%)	Main Effect
Sp_{O_2}, %	84.8 (5.4)†	97.3 (1.2)	97.9 (0.9)	<0.001
Heart rate, beats/min	64 (8)*	58 (8)	57 (7)	<0.05
Cardiac output, l/min	6.0 (0.8)	5.4 (0.9)	5.5 (1.6)	NS

Values are means (SD). Sp_{O_2}, arterial oxygen saturation by pulse oximetry; NS, not significant. Significant difference from normoxia and hyperoxia: *$P < 0.05$, †$P < 0.001$ on post hoc test.

Fig. 1. Representative magnetic resonance (MR) lung images from the 2 anatomic planes (sagittal and coronal) studied. Intersections of each plane with the other plane are indicated by long white lines (*left*). Short, solid white bar represents a 3-cm scale. *A1* and *A2* represent perfusion measured by arterial spin labeling (ASL), where the signal intensity is proportional to perfusion (ml blood$\cdot$min$^{-1}\cdot$cm^3 lung^{-1}). *B1* and *B2* represent proton density measured by fast low-angle shot (FLASH), where the signal intensity is proportional to proton density (g water/cm^3). *C1* and *C2* are density-normalized perfusion calculated by division of the ASL image by the FLASH image (ml$\cdot$min$^{-1}\cdot$g^{-1}). Density-normalized perfusion represents the perfusion per gram of lung water, which is from tissue and blood combined.
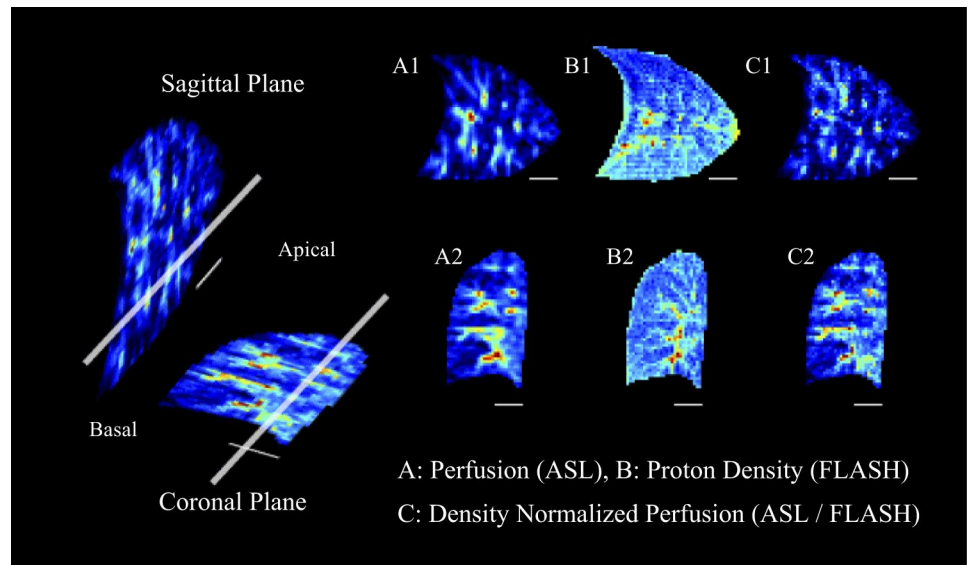
cant effect on pulmonary blood flow heterogeneity in the healthy supine lung. In fact, contrary to our hypotheses, there was a tendency for some measures of blood flow heterogeneity to be more uniform in hypoxia and unchanged in hyperoxia. These findings are in keeping with previous studies, which have suggested a predominant contribution of vascular structure to pulmonary blood flow heterogeneity in both animal (2, 16, 18, 26) and human (7) lungs. For example, microsphere studies in both supine pigs (27) and prone dogs (32) during hyperoxia do not show significant change in perfusion heterogeneity compared with normoxia. Similarly, in a bilateral ventilation study in dogs (35) in which the left lung was ventilated with hypoxic inspiratory gas and the right lung simultaneously received hyperoxic gas, there was no alteration of regional distribution of pulmonary blood flow in the hyperoxic side of lung. In keeping with the present study, Glenny and his coworkers (20) also showed that pulmonary perfusion heterogeneity (measured by relative dispersion) was not altered in baboon lung by administration of prostacyclin (PGI$_2$), which acts to reduce pulmonary vasomotor tone. Despite these findings, which suggest that alterations in regional vasomotor tone by hyperoxia or receptor blockade do not have a significant effect on pulmonary perfusion heterogeneity in the normal lung, there is also some evidence to the contrary. For example Melsom et al. (36) observed that hyperoxia (F$_{IO_2}$ = 0.40)

altered the regional distribution of pulmonary perfusion compared with normoxia and decreased the correlation in flow between identical locations in sheep lung under the two conditions. This effect was only transiently observed after 10-min exposure to hyperoxia and disappeared by 150 min.

In the present study, hypoxia also did not cause any alterations in pulmonary blood flow heterogeneity. Importantly, these findings are consistent with our previous work (28) in which only subjects with a history of high-altitude pulmonary edema (HAPE) showed significant increase in pulmonary blood flow heterogeneity in response to hypoxia. In subjects without a history of HAPE, perfusion heterogeneity did not change significantly, although as with the present study there was a tendency for blood flow to become slightly more uniform in response to 12.5% oxygen (28). However, this finding is not universally reported by others (11). The effects of hypoxia on pulmonary blood flow heterogeneity have also been investigated with animal models such as pigs (27, 45) and dogs (32). However, the different effects of hypoxia on pulmonary blood flow heterogeneity need to be evaluated considering not only the differing oxygen concentrations but also differences in posture and species. Characteristics of both pulmonary blood flow and the response to hypoxia are known to be different between postures in humans (38, 40, 42) and animals (2, 16, 17). For example, in pigs, pulmonary blood flow heterogeneity

Fig. 2. Effect of 3 different inspired oxygen concentrations on proton density (*A*) and density-normalized perfusion (*B*). Although mean proton density was greater in the coronal than the sagittal plane, reflecting the dependent location of the coronal plane, these changes did not reach statistical significance. Mean density-normalized perfusion in the sagittal plane was significantly greater than in the coronal plane. Neither mean proton density (*A*) nor mean density-normalized perfusion (*B*) was significantly changed by the different concentrations of inspired oxygen. NS, not significant. *$P < 0.05$.
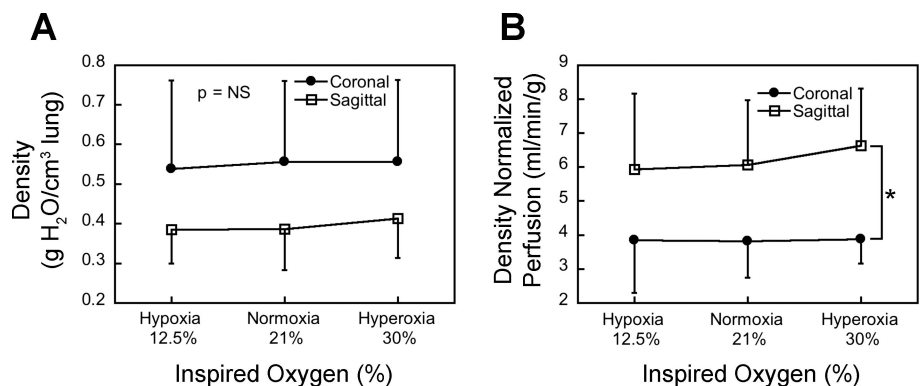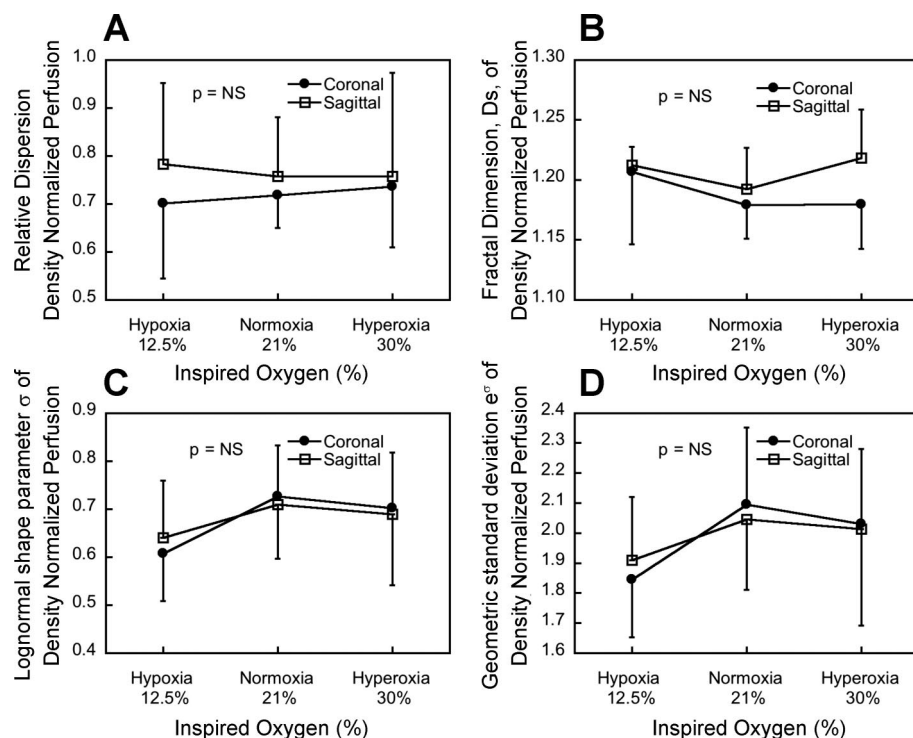
Fig. 3. Effect of 3 different inspired oxygen concentrations on pulmonary blood flow heterogeneity. Relative dispersion (A), fractal dimension (D_s, B), shape parameter (C), and geometric standard deviation (e^σ, D) of density-normalized perfusion were not significantly different between sagittal and coronal planes and were not changed by inspired oxygen concentrations.

measured by relative dispersion decreased during hypoxia (27) when the pig was supine but not in the prone posture (45). In the human lung, little difference in pulmonary blood flow heterogeneity between prone and supine postures (38, 42) has been reported, although this has not always been found (40). However, the human lung differs from animal lungs in that the active posture of humans is mainly upright whereas the usual

Fig. 4. Effect of different oxygen concentrations on vertical distribution of density-normalized perfusion. Density-normalized perfusion in the middle region was significantly greater than in either the dependent or the nondependent region (*P < 0.05) across the 3 different inspired oxygen concentrations. Inspired oxygen concentration did not significantly affect the vertical distribution of density-normalized perfusion, suggesting that on a gross scale the internal distribution of density-normalized perfusion was independent of inspired oxygen concentration. There was also no significant interaction effect between the 3 regions and inspired oxygen concentration ($P = 0.51$). $F_{I_{O_2}}$, inspired O_2 fraction.

posture of most animals is prone, and this may account for some of the difference. Moreover, differences in the pulmonary vascular response of the species studied may also contribute to the differing responses between studies. The pig is well known for a brisk hypoxic response, but, by contrast, the dog is known to have a minimal pulmonary vascular response to hypoxia (47).

Redistribution of pulmonary blood flow. One of the notable effects of hypoxia in the lung is an increase in pulmonary vascular resistance (10) and pulmonary artery pressure (12, 37) as a result of hypoxic pulmonary vasoconstriction. Because of the increase in pulmonary artery pressure and heterogeneous distribution of hypoxic pulmonary vasoconstriction throughout the lung, pulmonary blood flow distribution is known to be altered on a gross scale in both animal (27, 32, 45) and HAPE-susceptible human (22) lungs. The site of redistribution and recruitment is in the capillary bed (23, 49), which acts to increase diffusing capacity (8) via an increase in the gas exchange surface area (9). In our study, vertical redistribution of pulmonary blood flow (toward the anterior part of the lung in the supine posture) as a result of hypoxia-induced increases in pulmonary arterial pressure was not observed (Fig. 4). In the supine posture, the vertical height of the lung is ∼15 cm and almost 50% of lung is below the left atrium (13). Assuming the baseline pulmonary arterial pressure is 10–13 mmHg (12, 37), this leads to the conclusion that the human lung in a supine posture is almost all under zone 3 conditions (50). Thus even if pulmonary artery pressure increased to ∼25 mmHg, little effect would be expected on the vertical distribution of pulmonary blood flow. Hanaoka et al. (22) reported that pulmonary blood flow in the supine posture was shifted from basal to apical lung regions during hypoxia in HAPE-susceptible subjects but not in normal subjects, consistent with data from the present study. In animal studies, Capen and Wagner (9) reported that hypoxia-induced recruitment redistributed pulmo-

nary blood flow toward the upper lung in dogs, causing an increase in gas exchange surface area. A similar increase in regional pulmonary circulation to upper lung regions has also been reported in sheep (39). Those earlier studies concluded that the increase in pulmonary artery pressure increased flow against the vertical hydrostatic pressure gradient. However, in microsphere studies of dogs and pigs, regardless of species and posture, it has been shown that hypoxia redistributes pulmonary blood flow to the dorsal caudal lung, which is the most nondependent lung region in the normal awake quadruped posture (27, 32, 45).

Indexes of pulmonary blood flow heterogeneity. Relative dispersion showed no significant change between different inspired oxygen levels ($P = 0.97$; Fig. 3A), but the shape parameter and geometric standard deviation showed a tendency for pulmonary perfusion to become more uniform ($P = 0.07$ and $P = 0.11$, respectively; Fig. 3, C and D) and D_s to be more heterogeneous ($P = 0.07$; Fig. 3B) during hypoxia. Although relative dispersion, shape parameter, and geometric standard deviation are global scales of heterogeneity of blood flow, because of the long tail characteristics of log normal distributions, the shape parameter and geometric standard deviation are relatively insensitive to high signal representing blood flow in large vessels. The tendency of the shape parameter and geometric standard deviation to become somewhat more uniform in hypoxia despite little change in relative dispersion implies that blood flow in the small vessels becomes more uniform during hypoxia. This would be expected from hypoxia-induced vascular recruitment (23). Moreover, unlike the spatially independent nature of the other indexes, D_s represents the regional self-similarity of pulmonary blood flow distribution as a function of the scale of resolution (21). The trend of increasing D_s in hypoxia implies a more random regional distribution of pulmonary blood flow. Thus, in light of these findings, hypoxia may have caused pulmonary blood flow in poorly perfused regions to become more uniform, but spatial relocation of pulmonary blood flow may have occurred randomly.

Image planes. Although there was a trend for mean proton density to be greater in the coronal than the sagittal plane, these differences were not statistically significant (Fig. 2A). We selected the coronal imaging slices in a plane that encompassed the posterior one-third of the aorta (see Fig. 1), which were located in the relatively dependent part of the lung where proton density is high (6, 29). However, the sagittal plane encompasses all of the gravitational planes, and consequently the proton density, which varies with height from the most dependent lung, is averaged over the vertical height. Thus, depending on the relative dependent location of the coronal plane, density in this plane may be greater than the average of the sagittal plane. However, mean density-normalized perfusion in the sagittal plane was significantly greater than in the coronal plane (Fig. 2B), which also can be explained by the location of the image slices. In the most dependent part of lung, increased tissue density compresses extra-alveolar vessels, resulting in increased resistance (so-called zone 4) (30) and reducing flow.

Critique of methods. Our study focused solely on the perfusion side of pulmonary gas exchange. Clearly, gas exchange depends on both ventilation and perfusion. However, the change in distribution of ventilation due to different concentrations of oxygen is known to be much less than the change in perfusion (36). One issue that needs to be addressed is whether this study had adequate statistical power to support the conclusion reached, particularly in light of the small number of subjects studied. The repeated-measures design of this study, in which each subject acts as his/her own control, combined with a very high reliability of our measurement of perfusion heterogeneity (28), ensures excellent statistical power to detect a difference in perfusion heterogeneity with the different interventions, even if none was observed in the present study. For example, in order for the observed difference in relative dispersion of 0.74 and 0.76 between normoxia and hyperoxia to be statistically significant (if it in fact was) at $P < 0.05$, post hoc power calculations reveal that at least 200 subjects would be required. Thus any difference is biologically very small.

We did not monitor arterial CO_2 during our studies, which might be expected to have a confounding effect since hypercapnia has a vasoconstrictive stimulus on the pulmonary circulation. However, within the physiologically appropriate range (30–40 mmHg) the decrease in pulmonary blood flow due to hypercapnia is <5% (3). Thus the contribution of CO_2 tension (P_{CO_2}) to hypoxic pulmonary vasoconstriction is a very minor effect compared with that of alveolar hypoxia. In addition, in a study in which subjects lay quietly supine breathing the same gas mixtures as the present study, arterial P_{CO_2} (Pa_{CO_2}) showed minimal changes [$F_{IO_2} = 0.125$, $Pa_{CO_2} = 36.4(1.7)$ mmHg; $F_{IO_2} = 0.21$, $Pa_{CO_2} = 38.7(1.5)$ mmHg; $F_{IO_2} = 0.3$, $Pa_{CO_2} = 38.4(2.9)$ mmHg]. Thus the effect of the small alteration of Pa_{CO_2} is physiologically unimportant in this context.

This study also could have been strengthened if measurements of pulmonary artery pressure to document the extent of hypoxic pulmonary vasoconstriction were acquired. Unfortunately, the MRI techniques to measure pulmonary arterial pressure are unreliable (44), and Swan-Ganz catheters are a contraindication to MRI scanning. Noninvasive measurements such as echocardiography would require interrupting the study by taking a subject out of the scanner (and indeed out of the scanner room). Movement of the subject would risk misregistration of the images, introducing a source of significant error. It is possible that that our subjects had exceptionally modest pulmonary vascular responses to hypoxia. However, since an increase in pulmonary artery pressure with alveolar hypoxia has been reported in virtually all normal subjects (12, 37), we feel confident that our subjects had at least a small response to hypoxia. Another possibility is that the lack of significant findings is due to a lack of sensitivity of our measurements. However, our technique has been shown in the past to be highly sensitive to interventions affecting pulmonary perfusion; thus we do not think that the lack of changes in the present study is due to lack of sensitivity of the technique. For example, the relative dispersion has also been shown to increase with age by ~0.1 per decade of age (33), consistent with the well-documented changes in pulmonary function with aging. Also, 1 h of 30° head-down tilt, which increases pulmonary vascular pressures, also caused a significant increase in pulmonary blood flow heterogeneity measured by relative dispersion (25).

Like all measurements, our techniques have limitations. We have attempted to correct for technical matters such as coil inhomogeneity and absolute calibration by correcting for coil

inhomogeneity profile and incorporating reference phantoms in our imaging protocols. Our measurements are, however, limited by our ability to acquire data during a breath hold and also by the need to acquire the perfusion and density images during separate breath holds, which may introduce some error into these measurements, although visual inspection of diaphragmatic position indicated reproducible breath-hold volumes. Furthermore, our density measurements image only free protons (essentially water), and so our distribution of density may be incorrect if lung tissue that does not contribute to the MRI signal is distributed differently to water in the lung. Finally, our study examined only the right lung, to avoid imaging artifacts from the heart on the left side of the chest. We do not, however, see any reason to suspect a different result for the left lung in terms of the effect of hypoxia and hyperoxia.

Conclusion. We conclude that in supine normoxic humans, the heterogeneity of pulmonary blood flow observed within an isogravitational plane is not due to hypoxic pulmonary vasoconstriction, and gross redistribution of pulmonary blood flow during both hypoxia and hyperoxia was also not found. Thus the results of this study suggest that the observed heterogeneity of pulmonary blood flow is structural or gravitational in nature and that dynamic vascular factors play a limited role.

ACKNOWLEDGMENTS

GRANTS

REFERENCES

1. **Akça O, Podolsky A, Eisenhuber E, Panzer O, Hetz H, Lampl K, Lackner F, Wittmann K, Grabenwoeger F, Kurz A, Schultz A, Negishi C, Sessler D.** Comparable postoperative pulmonary atelectasis in patients given 30% or 80% oxygen during and 2 hours after colon resection. *Anesthesiology* 91: 991–998, 1999.
2. **Altemeier W, McKinney S, Krueger M, Glenny R.** Effect of posture on regional gas exchange in pigs. *J Appl Physiol* 97: 2104–2111, 2004.
3. **Barer G, Howard P, Shaw J.** Stimulus-response curves for the pulmonary vascular bed to hypoxia and hypercapnia. *J Physiol* 211: 139–155, 1970.
4. **Bolar D, Levin D, Hopkins S, Frank L, Liu T, Wong E, Buxton R.** Quantification of regional pulmonary blood flow using ASL-FAIRER. *Magn Reson Med* 55: 1308–1317, 2006.
5. **Brimioulle S, Lejeune P, Vachiéry J, Delcroix M, Hallemans R, Leeman M, Naeije R.** Stimulus-response curve of hypoxic pulmonary vasoconstriction in intact dogs: effects of ASA. *J Appl Physiol* 77: 476–480, 1994.
6. **Brudin LH, Rhodes CG, Valind SO, Wollmer P, Hughes JM.** Regional lung density and blood volume in nonsmoking and smoking subjects measured by PET. *J Appl Physiol* 63: 1324–1334, 1987.
7. **Burrowes K, Tawhai M.** Computational predictions of pulmonary blood flow gradients: gravity versus structure. *Respir Physiol Neurobiol* 154: 515–523, 2006.
8. **Capen R, Latham L, Wagner WJ.** Diffusing capacity of the lung during hypoxia: role of capillary recruitment. *J Appl Physiol* 50: 165–171, 1981.
9. **Capen R, Wagner WJ.** Intrapulmonary blood flow redistribution during hypoxia increases gas exchange surface area. *J Appl Physiol* 52: 1575–1580, 1982.
10. **Dawson C.** Role of pulmonary vasomotion in physiology of the lung. *Physiol Rev* 64: 544–616, 1984.
11. **Dehnert C, Risse F, Ley S, Kuder T, Buhmann R, Puderbach M, Menold E, Mereles D, Kauczor H, Bärtsch P, Fink C.** Magnetic resonance imaging of uneven pulmonary perfusion in hypoxia in humans. *Am J Respir Crit Care Med* 174: 1132–1138, 2006.
12. **Doyle J, Wilson J, Warren J.** The pulmonary vascular responses to short-term hypoxia in human subjects. *Circulation* 5: 263–270, 1952.
13. **Friedman P, Peters R, Botkin M, Brimm J, Meltvedt R.** Estimation of the volume of lung below the left atrium using computed tomography. *Crit Care Med* 14: 182–187, 1986.
14. **Gatehouse P, Keegan J, Crowe L, Masood S, Mohiaddin R, Kreitner K, Firmin D.** Applications of phase-contrast flow and velocity imaging in cardiovascular MRI. *Eur Radiol* 15: 2172–2184, 2005.
15. **Glenny R, Bernard S, Neradilek B, Polissar N.** Quantifying the genetic influence on mammalian vascular tree structure. *Proc Natl Acad Sci USA* 104: 6858–6863, 2007.
16. **Glenny R, Bernard S, Robertson H, Hlastala M.** Gravity is an important but secondary determinant of regional pulmonary blood flow in upright primates. *J Appl Physiol* 86: 623–632, 1999.
17. **Glenny R, Lamm W, Albert R, Robertson H.** Gravity is a minor determinant of pulmonary blood flow distribution. *J Appl Physiol* 71: 620–629, 1991.
18. **Glenny R, Polissar L, Robertson H.** Relative contribution of gravity to pulmonary perfusion heterogeneity. *J Appl Physiol* 71: 2449–2452, 1991.
19. **Glenny R, Robertson H.** Fractal properties of pulmonary blood flow: characterization of spatial heterogeneity. *J Appl Physiol* 69: 532–545, 1990.
20. **Glenny R, Robertson H, Hlastala M.** Vasomotor tone does not affect perfusion heterogeneity and gas exchange in normal primate lungs during normoxia. *J Appl Physiol* 89: 2263–2267, 2000.
21. **Glenny RW.** Heterogeneity in the lung: concepts and measures. In: *Complexity in Structure and Function in the Lung*, edited by Hlastala MP, Robertson HT. New York: Dekker, 1998, p. 571–609.
22. **Hanaoka M, Tanaka M, Ge R, Droma Y, Ito A, Miyahara T, Koizumi T, Fujimoto K, Fujii T, Kobayashi T, Kubo K.** Hypoxia-induced pulmonary blood redistribution in subjects with a history of high-altitude pulmonary edema. *Circulation* 101: 1418–1422, 2000.
23. **Hanson W, Emhardt J, Bartek J, Latham L, Checkley L, Capen R, Wagner WJ.** Site of recruitment in the pulmonary microcirculation. *J Appl Physiol* 66: 2079–2083, 1989.
24. **Hatabu H, Alsop D, Listerud J, Bonnet M, Gefter W.** T2* and proton density measurement of normal human lung parenchyma using submillisecond echo time gradient echo magnetic resonance imaging. *Eur J Radiol* 29: 245–252, 1999.
25. **Henderson A, Levin D, Hopkins S, Olfert I, Buxton R, Prisk G.** Steep head-down tilt has persisting effects on the distribution of pulmonary blood flow. *J Appl Physiol* 101: 583–589, 2006.
26. **Hlastala M, Glenny R.** Vascular structure determines pulmonary blood flow distribution. *News Physiol Sci* 14: 182–186, 1999.
27. **Hlastala M, Lamm W, Karp A, Polissar N, Starr I, Glenny R.** Spatial distribution of hypoxic pulmonary vasoconstriction in the supine pig. *J Appl Physiol* 96: 1589–1599, 2004.
28. **Hopkins S, Garg J, Bolar D, Balouch J, Levin D.** Pulmonary blood flow heterogeneity during hypoxia and high-altitude pulmonary edema. *Am J Respir Crit Care Med* 171: 83–87, 2005.
29. **Hopkins S, Henderson A, Levin D, Yamada K, Arai T, Buxton R, Prisk G.** Vertical gradients in regional lung density and perfusion in the supine human lung: the Slinky effect. *J Appl Physiol* 103: 240–248, 2007.
30. **Hughes JM, Glazier JB, Maloney JE, West JB.** Effect of lung volume on the distribution of pulmonary blood flow in man. *Respir Physiol* 4: 58–72, 1968.
31. **Jones A, Hansell D, Evans T.** Pulmonary perfusion in supine and prone positions: an electron-beam computed tomography study. *J Appl Physiol* 90: 1342–1348, 2001.
32. **Lamm W, Starr I, Neradilek B, Polissar N, Glenny R, Hlastala M.** Hypoxic pulmonary vasoconstriction is heterogeneously distributed in the prone dog. *Respir Physiol Neurobiol* 144: 281–294, 2004.
33. **Levin D, Buxton R, Spiess J, Arai T, Balouch J, Hopkins S.** Effects of age on pulmonary perfusion heterogeneity measured by magnetic resonance imaging. *J Appl Physiol* 102: 2064–2070, 2007.
34. **Limpert E, Stahel W, Abbt M.** Log-normal distributions across the sciences: keys and clues. *Bioscience* 51: 341–352, 2001.
35. **Mann C, Domino K, Walther S, Glenny R, Polissar N, Hlastala M.** Redistribution of pulmonary blood flow during unilateral hypoxia in prone and supine dogs. *J Appl Physiol* 84: 2010–2019, 1998.
36. **Melsom M, Flatebø T, Nicolaysen G.** Hypoxia and hyperoxia both transiently affect distribution of pulmonary perfusion but not ventilation in awake sheep. *Acta Physiol Scand* 166: 151–158, 1999.

37. **Motley HL, Cournand A, Werko L, Himmelsten A, Dresdale D.** The influence of short periods of induced acute anoxia upon pulmonary artery pressures in man. *Am J Physiol* 150: 315, 1947.

38. **Musch G, Layfield J, Harris R, Melo M, Winkler T, Callahan R, Fischman A, Venegas J.** Topographical distribution of pulmonary perfusion and ventilation, assessed by PET in supine and prone humans. *J Appl Physiol* 93: 1841–1851, 2002.

39. **Neumann P, Kivlen C, Johnson A, Minnear F, Malik A.** Effect of alveolar hypoxia on regional pulmonary perfusion. *J Appl Physiol* 56: 338–342, 1984.

40. **Nyrén S, Mure M, Jacobsson H, Larsson S, Lindahl S.** Pulmonary perfusion is more uniform in the prone than in the supine position: scintigraphy in healthy humans. *J Appl Physiol* 86: 1135–1141, 1999.

41. **Peake M, Harabin A, Brennan N, Sylvester J.** Steady-state vascular responses to graded hypoxia in isolated lungs of five species. *J Appl Physiol* 51: 1214–1219, 1981.

42. **Prisk G, Yamada K, Henderson A, Arai T, Levin D, Buxton R, Hopkins S.** Pulmonary perfusion in the prone and supine postures in the normal human lung. *J Appl Physiol* 103: 883–894, 2007.

43. **Robertson H, Hlastala M.** Microsphere maps of regional blood flow and regional ventilation. *J Appl Physiol* 102: 1265–1272, 2007.

44. **Roeleveld R, Marcus J, Boonstra A, Postmus P, Marques K, Bronzwaer J, Vonk-Noordegraaf A.** A comparison of noninvasive MRI-based methods of estimating pulmonary artery pressure in pulmonary hypertension. *J Magn Reson Imaging* 22: 67–72, 2005.

45. **Starr I, Lamm W, Neradilek B, Polissar N, Glenny R, Hlastala M.** Regional hypoxic pulmonary vasoconstriction in prone pigs. *J Appl Physiol* 99: 363–370, 2005.

46. **Swenson E, Domino K, Hlastala M.** Physiological effect of oxygen and carbon dioxide on VA/Q heterogeneity. In: *Complexity in Structure and Function in the Lung*, edited by Hlastala M, Robertson HT. New York: Dekker, 1998, p. 511–547.

47. **Tucker A, Rhodes J.** Role of vascular smooth muscle in the development of high altitude pulmonary hypertension: an interspecies evaluation. *High Alt Med Biol* 2: 173–189, 2001.

48. **Wagner P, Laravuso R, Uhl R, West J.** Continuous distributions of ventilation-perfusion ratios in normal subjects breathing air and 100 per cent O₂. *J Clin Invest* 54: 54–68, 1974.

49. **Wagner WJ, Latham L.** Pulmonary capillary recruitment during airway hypoxia in the dog. *J Appl Physiol* 39: 900–905, 1975.

50. **West J, Dollery C, Naimark A.** Distribution of blood flow in isolated lung: relation to vascular and alveolar pressures. *J Appl Physiol* 19: 713–724, 1964.